Commun. Comput. Phys.
doi: 10.4208/cicp.250913.240314a

Vol. **16**, No. 3, pp. 781-798
September 2014

# Finding Critical Nuclei in Phase Transformations by Shrinking Dimer Dynamics and its Variants

Lei Zhang[1], Jingyan Zhang[2] and Qiang Du[2,3,*]

[1] *Beijing International Center for Mathematical Research, Peking University, Beijing 100871, China.*
[2] *Department of Mathematics, Pennsylvania State University, PA 16802, USA.*
[3] *Beijing Computational Science Research Center, Beijing, 100084, China.*

Received 25 September 2013; Accepted (in revised version) 24 March 2014

Communicated by Long-Qing Chen

Available online 4 July 2014

**Abstract.** We investigate the critical nuclei morphology in phase transformation by combining two effective ingredients, with the first being the phase field modeling of the relevant energetics which has been a popular approach for phase transitions and the second being shrinking dimer dynamics and its variants for computing saddle points and transition states. In particular, the newly formulated generalized shrinking dimer dynamics is proposed by adopting the Cahn-Hilliard dynamics for the generalized gradient system. As illustrations, a couple of typical cases are considered, including a generic system modeling heterogeneous nucleation and a specific material system modeling the precipitate nucleation in FeCr alloys. While the standard shrinking dimer dynamics can be applied to study the non-conserved case of generic heterogeneous nucleation directly, the generalized shrinking dimer dynamics is efficient to compute precipitate nucleation in FeCr alloys due to the conservation of concentration. Numerical simulations are provided to demonstrate both the complex morphology associated with nucleation events and the effectiveness of generalized shrinking dimer dynamics based on phase field models.

**AMS subject classifications**: 37M05, 49K35, 37N30, 34K28, 65P99

**Key words**: Critical nucleus, phase field models, saddle point, shrinking dimer dynamics, heterogeneous nucleation, precipitate nucleation, phase transformation.

## 1 Introduction

Many material processes start with the nucleation of nanoscale nuclei of new phase particles, and followed by growth and particle impingement or coarsening. Nucleation in

*Corresponding author. *Email addresses:* zhangl@math.pku.edu.cn (L. Zhang), j_zhang@math.psu.edu (J. Y. Zhang), qdu@math.psu.edu (Q. Du)

 ©2014 Global-Science Press

phase transformations is often viewed as a difficult process to study experimentally since the nucleation process is a rare event and the critical nucleus only appears transiently. It also poses a modeling challenge given the complex energy landscape and material heterogeneities. Finding critical nucleus configuration computationally has attracted much attention in recent years [1–6]. There have been much studies on the homogeneous nucleation through both classical nucleation theory and non-classical diffuse interface theory [1, 4, 6] which utilizes the phase field approach to model the nucleation and microstructure evolution.

Nucleation of a new phase requires overcoming a minimum thermodynamic barrier. A critical nucleus is defined as the order parameter or composition fluctuation having the minimum free energy increase among all fluctuations which lead to nucleation, i.e., the saddle point configuration along the minimum energy path between the initial metastable phase and the final equilibrium phase. Thus, finding saddle points (transition states) of an energy landscape is critical to the study of rare thermally-activated transitions between different equilibria and metastable states associated with the total free energy landscape. There have been extensive studies of numerical algorithms for computing saddle point including chain-of-state methods such as nudged elastic band [7] and string method [8, 9] which provides the minimum energy path containing the desired saddle point and surface-walking methods such as gentlest ascent method [10, 11], dimer method [12] and shrinking dimer dynamics [13], and so on [14]. During the phase transformation, the computation of saddle points is often subject to one or more constraints, such as precipitation in a supersaturated solid or liquid solution. It is thus necessary to develop algorithms to compute constrained saddle point by overcoming difficulties caused by both the unstable nature of saddle points and the complications due to constraints. To complement unconstrained algorithms, constrained string method was developed as a chain-of-state method to find constrained minimum energy path [15] and constrained shrinking dimer dynamics has also been proposed recently as a surface-walking method to search index-1 saddle point on a constrained manifold [16].

In terms of applying saddle point search algorithms to the nucleation problem, much of the focus has so far been on the homogeneous nucleation and the corresponding morphology of critical nuclei. For instance, the phase field approach and the minimax algorithm have been used to predict the morphology of critical nucleus in solids by taking into account both interfacial anisotropy and long range elastic interactions [4, 17, 18]. Other successful applications include finding both critical nucleus and equilibrium precipitate simultaneously in solids [6, 19], incorporating diffuse-interface critical nuclei in phase field simulation [20], using phase-field-crystal model to find critical nuclei for homogeneous nucleation [21] and finding the transition pathway of ordered phases in block copolymers [5]. As most of the nucleation events in practice are not homogeneous due to the presence of grain boundaries or crystal lattice defects, heterogeneous nucleation often occurs at preferential sites [22, 23], thus leading to further complications to the critical nuclei morphology.

In this paper, we illustrate the effectiveness of coupling the shrinking dimer dynamics

(SDD) and its extension - generalized shrinking dimer dynamics (GSDD) with phase field models to simulate the critical nucleation. Our work includes both new methodology and new applications. For the latter, we consider a couple of typical cases that represent in one case morphology of critical nuclei due to material heterogeneities in a generic system, and in the other case the morphology in a real material system associated with a specific binary alloy. To be more specific, in the first case, we model heterogeneous nucleation by introducing a spatially varying energy density, while in the second case, we study the precipitate nucleation in FeCr alloys. We examine how the critical nuclei morphology is affected by various factors such as driving force, level of inhomogeneity, interfacial anisotropy, and complex geometries. As for the methodology, the GSDD is a new formulation and an extension of the SDD which provides the dimer dynamics analog of the generalized gradient dynamics associated with the free energy. Such a generalization allows a natural incorporation of the conservation conditions, in the same spirit as the Cahn-Hilliard dynamics which is an example of the conserved gradient dynamics. This interesting analogy is provided for the first time here, along with numerical comparisons between the different formulations. In numerical simulations, the standard SDD is applied to study the first non-conserved case, while the second conserved case requires the use of GSDD or alternatively constrained shrinking dimer dynamics (CSDD). As demonstrated through extensive numerical experiments, SDD and GSDD are able to efficiently find critical nuclei and allow us to make interesting observations on phase transformation.

The rest of this paper is organized as follows: In Section 2, we describe the phase field model of nucleation and numerical algorithms of SDD and CSDD. We also introduce the GSDD as a generalization of the previously proposed SDD and CSDD. We then apply the SDD and GSDD to study critical nucleation in Section 3 which includes a generic example of heterogeneous nucleation and a more realistic example of nucleation in FeCr alloys in both two and three dimensional spaces. Final conclusions are given in Section 4.

## 2 Method

### 2.1 Phase field model

Following the seminal work by Cahn and Hilliard [1], phase field (diffuse interface) models have been employed to study nucleation and microstructure evolution in phase transformation. A phase field variable $\eta$ is often used to describe the compositional/structural difference between the parent phase and nucleation phase. Then the total free energy of the binary system is formulated as

$$E(\eta)=\int_\Omega \Big(\frac{1}{2}|M\nabla\eta|^2+f(\eta)\Big)d\mathbf{x}, \tag{2.1}$$

where the gradient coefficient $M$ can be used to reflect the interfacial energy anisotropy and the local free energy density $f=f(\eta)$ is a double-well energy potential. An example

of $f=f(\eta)$ is

$$f(\eta)=\frac{\eta^4}{4}-\frac{\eta^2}{2}+\rho\frac{\eta^3-3\eta}{4}, \tag{2.2}$$

where two energy wells are located at $\eta=1$ and $-1$, and the driving force $\rho$ determines the energy difference between two wells.

For solid state phase transformation, to account for the long-range elastic interactions in solids for an arbitrary distribution of $\eta$, in the case that the elastic modulus is anisotropic but homogeneous, the elastic energy should be taken into consideration [4] based on the microelasticity theory [24].

The critical nucleus can be identified as the saddle-point solution of the Euler-Lagrange equation by taking the functional derivative of $E_{total}(\eta)$. In practice, the phase field variable $\eta$ may be subject to additional physical constraints. For instance, the mass conservation:

$$\int_\Omega(\eta(\mathbf{x})-\eta_0)d\mathbf{x}=0,$$

with an average composition $\eta_0$.

## 2.2 Shrinking dimer dynamics

Given an energy functional $E=E(x)$ on a Hilbert space $\mathcal{H}$, we let $\nabla E(x)$ denote the gradient of $E$ at $x\in\mathcal{H}$ defined in the Frechet sense with respect to an inner product (duality pairing) in a space $\mathcal{L}$ containing $\mathcal{H}$, and $H_E(x)$ be the Hessian operator of $E$ at $x\in\mathcal{H}$. Such abstract functional analytic setting will be illustrated through concrete examples in later discussions.

As in [12,13], a dimer consists of a pair of points $x_1$ and $x_2$ in $\mathcal{H}$ with the dimer length $l=\|x_1-x_2\|$. The dimer orientation is given by a unit vector $v$ so that $x_1-x_2=lv$. The (rotating) center of the dimer is defined by

$$x_\alpha=(1-\alpha)x_1+\alpha x_2, \tag{2.3}$$

where the parameter $\alpha\in[0,1]$ gives us the freedom to choose a point other than the geometric center (the midpoint of the dimer corresponding to $\alpha=1/2$). For notation convenience, let

$$F_i=-\nabla E(x_i),\quad i=1,2,\quad\text{and}\quad F_\alpha=-\nabla E(x_\alpha) \tag{2.4}$$

be natural forces at the two endpoints and the rotating center of the dimer.

Proposed in [13] as a dynamic system for index-1 saddle point search, the SDD is given by

$$\begin{cases}\mu_1\dot{x}_\alpha=(I-\sigma vv^T)((1-\alpha)F_1+\alpha F_2),\\ \mu_2\dot{v}=(I-vv^T)\dfrac{(F_1-F_2)}{l},\\ \mu_3\dot{l}=-\nabla V(l),\end{cases} \tag{2.5}$$

where $\mu_1,\mu_2,\mu_3$ are nonnegative relaxation constants. $\sigma$ is a constant scalar which is set to be $\sigma=2$ for index-1 saddle point computation. The notation $vv^T$ is interpreted as $vv^Ty=v^Tyv$ for any $v\in\mathcal{H}$ and $y\in\mathcal{H}^*$. An energy function $V(l)$ is used to control the dimer length $l$, and it is generally taken as a monotonically increasing function in $l$ such that $l\equiv 0$ is the unique critical point of $V=V(l)$. The initial condition of system (2.5) is chosen as $x_\alpha(0)=x_0$, $v(0)=v_0$, $l(0)=l_0>0$, $x_0,v_0\in\mathcal{H}$ with $\|v_0\|=1$ in $\mathcal{L}$.

As explained in [13], the first two equations of (2.5) represent the translation step and the rotation step, respectively, which essentially follow from the dimer method originally developed in [12]. The operator $I-\sigma vv^T=I-2vv^T$ is the Householder mirror reflection which reverses the component of the natural force along $v$ while $(I-vv^T)$ is a projection to keep $v$ of unit length. The third equation in (2.5) follows a gradient flow of $V(l)$ and allows the shrinking of the dimer length over time by forcing it to approach zero. The solution of the system (2.5) is expected to converge to an exact saddle point at the steady state, see [13] for detailed convergence analysis.

An explicit Euler method and a modified Euler scheme for SDD, which performs a normalization on $v$ at each step, have been studied for SDD [13]. To improve the stability and reduce the stiffness of the SDD system, semi-implicit splitting techniques can be introduced to the discrete SDD system to allow a larger time step size and obtain better error reduction [13].

Note that in the numerical implementation, we often take $\alpha=1/2$ in (2.5). The choice of spaces are such that $\mathcal{L}=L^2(\Omega)$, the standard space of square integrable functions in $\Omega$, and $\mathcal{H}=H^1(\Omega)$, the standard Sobolev space of functions in $L^2(\Omega)$ with their first order derivatives also in $L^2(\Omega)$. The normalization on $v$ is carried out at each step to explicitly guarantee the condition that $\|v^n\|_{L^2}=1$. The parameter $\delta$ is taken to further reduce the stiffness due to the nonlinear term, and we let $\delta=2$ in our implementation which is an effective choice related to the energy stable splitting of the commonly chosen double-well potential $(\eta^2-1)^2/4$, although the optimal choice of $\delta$ may depend on $\rho$ in general for the potential function in the form of (2.2) [25,26].

### 2.3 Constrained shrinking dimer dynamics

For some of the nucleation problems under consideration, the saddle point search is subject to certain constraints. In [16], a constrained shrinking dimer dynamics (CSDD) has been proposed to search for constrained index-1 saddle points on a potential energy surface subject to general equality constraints. For instance, without loss of generality, we consider the abstract setting where the index-1 saddle point of $E=E(x)$ is subject to the constraint:

$$G(x)=0, \tag{2.6}$$

where $G:\mathcal{H}\to\mathcal{B}$ is assumed to be a smooth operator from $\mathcal{H}$ to a Hilbert space $\mathcal{B}$. In particular, $G$ could be a scalar functional taking values in $\mathbb{R}$ which is the case used in this work.

To enforce the constraints, CSDD uses the projected natural force, which is the negative gradient force projected on the tangential hyperplane (space) of the constrained manifold:

$$P(G) := I - \nabla G^T[(\nabla G)^T \nabla G^T]^{-1}(\nabla G)^T, \tag{2.7}$$

where the constraints are assumed to be independent so that $(\nabla G)^T \nabla G^T$ is a positive definite operator with a well-defined inverse $[(\nabla G)^T \nabla G^T]^{-1}$.

With the above notation, the CSDD given in [16] has the following form:

$$\begin{cases} \mu_1 \dot{x}_\alpha = (I - \sigma v v^T)((1-\alpha)P(G_\alpha)F_1 + \alpha P(G_\alpha)F_2), \\ \mu_2 \dot{v} = (I - vv^T)[P(G_\alpha)F_1 - P(G_\alpha)F_2]/l + \beta \nabla G_\alpha^T, \\ \mu_3 \dot{l} = -\nabla V(l), \end{cases} \tag{2.8}$$

where $G_\alpha = G(x_\alpha) = G((2-\alpha)x_1 + (1-\alpha)x_2)$, and the relaxation constants $\mu_1, \mu_2, \mu_3$, the functional $E_l(l)$ are same as SDD. The constant scalar $\sigma$ is also set to be $\sigma = 2$. The initial condition of CSDD needs the following compatibility assumption:

$$G(x_0) = 0, \quad \|v_0\| = 1 \quad \text{and} \quad (\nabla G(x_0))^T v_0 = 0. \tag{2.9}$$

For general constraints, the Lagrange multiplier $\beta$ in (2.8) is used to enforce $(\nabla G(x))^T v = 0$. It has several formulations as presented in [16]. For linear constraints, it can be easily shown that $\beta = 0$. The CSDD in this case is then essentially the same as SDD except for the need to apply the projection $P(G_\alpha)$ on the forcing terms. In the numerical implementation of CSDD, one may apply an explicit time marching scheme like the forward Euler method. We may also derive a similar semi-implicit scheme as the one obtained for SDD to improve stability and ensure the convergence to the steady state.

### 2.4 Generalized shrinking dimer dynamics

As one of our goals here is to compute constrained saddle points based on the diffuse interface theory, it is well known that different types of dynamics can be used to study the transient behavior of the phase field variables, for example, the Allen-Cahn dynamics for nonconserved variables and Cahn-Hilliard dynamics for conserved variables. These dynamics all correspond to gradient flows of the diffuse interface energy, but with different choices of duality (inner product). The Allen-Cahn equation refers to the standard $L^2$ inner product while the Cahn-Hilliard equation uses the $H^{-1}$ inner product.

We note that the study of SDD can also be extended to incorporate the use of different inner products for defining the dynamic systems. The convergence analysis remains basically the same. For this reason, we now introduce a generalized shrinking dimer dynamics (GSDD) as follows:

$$\begin{cases} \mu_1 A \dot{x}_\alpha = (I - \sigma v v^T)((1-\alpha)P(G_\alpha)F_1 + \alpha P(G_\alpha)F_2), \\ \mu_2 \dot{v} = (I - vv^T)[P(G_\alpha)F_1 - P(G_\alpha)F_2]/l + \beta \nabla G_\alpha^T, \\ \mu_3 \dot{l} = -\nabla V(l), \end{cases} \tag{2.10}$$

where $A$ is a positive definite linear operators defined on $\mathcal{L}$ which are independent of $x$, $v$ and $l$, and for index-1 saddle point computation, we always take $\sigma=2$ so as to make $(I-\sigma vv^T)$ a Householder mirror reflection for $v$ satisfying $v^Tv=1$. The initial condition is naturally required to satisfy $v_0^Tv_0=1$ as before.

For the original CSDD, we have $A=\mathrm{I}$, the identity operator, then (2.10) reduces to exactly (2.8). In general function spaces, (2.10) represents a generalization of the CSDD as well the original SDD (if we have no constraints). For example, let

$$\mathcal{H}=\left\{u\in H^1(\Omega)\,|\,\int_\Omega u d\mathbf{x}=0\right\}$$

be the space of functions in the standard Sobolev space $H^1$ defined on a domain $\Omega$ having mean zero. Let $\Delta$ be the Laplacian operator, we may then take $A=(-\Delta)^{-1}$ for conserved dynamics. Since a constant function is in the kernel of $\Delta$, the resulting GSDD then provides a naturally conserved dynamics without the need to impose the additional conservation constraints as in the CSDD. This is analogous to the conserved Cahn-Hilliard gradient dynamics [1] (which can be obtained from the first equation of (2.10) by setting $\sigma=0$. In comparison, we notice that for $\sigma=0$, the first equations of the SDD and CSDD would then corresponds respectively to the Allen-Cahn dynamics and the conserved Allen-Cahn dynamics associated with the free energy functional.

Before we end the general discussions on the SDD types of methods, we note that the convergence analysis of GSDD (2.10) can be carried out in the same way as for the original SDD and CSDD [13,16]. We omit the details.

## 3 Application to nucleation

We now present examples that demonstrate the effectiveness of SDD and GSDD to model and simulate the nucleation events. We consider two typical cases that represent respectively a generic system with heterogeneities as well as a real material system associated with a specific binary alloy.

### 3.1 Heterogeneous nucleation

Heterogeneous nucleation occurs much more often than homogeneous nucleation, and it forms at preferential sites such as phase boundaries or surfaces. We may apply the SDD to compute critical nuclei with the phase field formulation of heterogenous nucleation that includes various crystalline effects (such as inhomogeneity, interfacial anisotropy, complex phase boundary, etc). In general, the causes of concentration inhomogeneity could be presence of structure defects, such as point defects, dislocations, twin and grain boundaries, cracks, and inhomogeneous inclusions, etc. The distributions of inhomogeneity can be described by stress-free strains or eigenstrains in the inhomogeneous elastic energy [27,28]. In order to illustrate the methods and the effects of inhomogeneities

without the need to carry out the calculation of elastic energy, we take a generic system as an illustration and adopt a phenomenological function to mimic the heterogeneous effects on the critical nuclei. The full account of inhomogeneous and anisotropic elastic energy can be considered by adopting approaches similar to those in earlier studies [19,27–29].

We consider the modification of the energy functional (2.1) by

$$E(\eta)=\int_\Omega \frac{\theta(\mathbf{x})}{2}\left[|M\nabla\eta(\mathbf{x})|^2+f(\eta(\mathbf{x}))\right]d\mathbf{x}, \tag{3.1}$$

where the function $\theta=\theta(\mathbf{x})$ represents the contributions from spatial inhomogeneities in the domain. The coefficient matrix $M$ is assumed to be a constant tensor modeling the interfacial anisotropy and the local free energy density $f(\eta)$ is same as (2.2).

We now consider a two dimensional sample, and choose

$$\theta(x,y)=\tanh^4\left(\frac{x+0.2}{0.01}\right),$$

for $(x,y)\in\Omega=[-1,1]^2$ with the gradient coefficient $M=0.0004\mathrm{I}$. Thus, the inhomogeneities are concentrated near a straight line $x=-0.2$ so that it is energetically favorable to have interfaces represented by $\eta$ align with the straight line $x=-0.2$.

First of all, we study the effect of the driving force on critical nuclei. We let the driving force $\rho$ change from 0.1,0.07,0.05 to 0.01 in (2.2) and compute a branch of critical nuclei. Fig. 1 contains the density plots of the phase field function $\eta=\eta(x,y)$ and those corresponding to the unstable directions. The plots clearly indicate that the driving force mostly affects the sizes of critical nuclei, but not their shapes. The unstable directions of critical nuclei indicate the growth directions of nuclei after nucleation. Effects of inhomogeneities are also evident. Without inhomogeneities, the nuclei are mostly circular, while with inhomogeneities concentrating on a straight line, the shape becomes semi-circular as part of the nucleus boundary falls on the line of inhomogeneities.

Next, we change the concentration of inhomogeneity from that on a straight line to that on a curve. We also use a parameter $\gamma$ to represent the intensity of inhomogeneities so that the function $\theta$ is modified by

$$\theta(x,y)=1-\gamma+\gamma\tanh^4\left(\frac{x+0.2\cos(\pi y)+0.2}{0.01}\right). \tag{3.2}$$

Numerical simulations show that the shape of critical nucleus has a circular form without inhomogeneity ($\gamma=0$) in Fig. 2(A). With the increase of inhomogeneity levels in Fig. 2(B-D), the critical nucleus changes its shape from circle to that bounded between a near circular arc and part of the curvy inhomogeneity (see Fig. 2(D)). It reveals that the morphology of critical nucleus strongly depends on inhomogeneous interface conditions.

To study effects of interfacial anisotropy on the shapes of critical nuclei, we take $M$ to be a diagonal matrix of the form

$$M=0.0004\begin{pmatrix} a & 0 \\ 0 & 1/a \end{pmatrix},$$

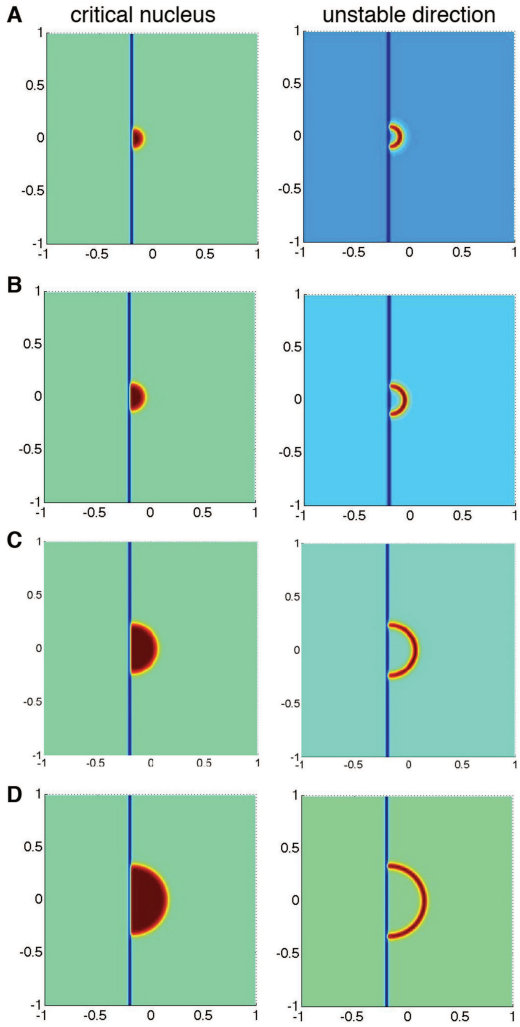


Figure 1: Critical nuclei and unstable directions near a straight line boundary having different driving force with (A) $\beta=0.1$, (B) $\beta=0.07$, (C) $\beta=0.05$, and (D) $\beta=0.01$.

and retain the same $\theta$ in (3.2) with $\gamma=0.1$.

In the presence of a curvy inhomogeneous boundary, we take $a=4,2,1,1/2$ and $1/4$ in Fig. 3(A-E), respectively. As expected, the critical nuclei take on shapes that depend on interfacial anisotropy. Unstable directions of critical nuclei also reveal how the growth direction changes after nucleation.

To further explore the complex geometric effects of inhomogeneities on the energy landscape and critical nuclei, we take a self-intersecting wavy curve corresponding to $\theta$ of the form

$$\theta(x,y)=\tanh^4\left(\frac{x+0.3\cos(\pi y-0.3)}{0.01}\right)\tanh^4\left(\frac{x-0.3\cos(\pi y-0.3)}{0.01}\right), \tag{3.3}$$

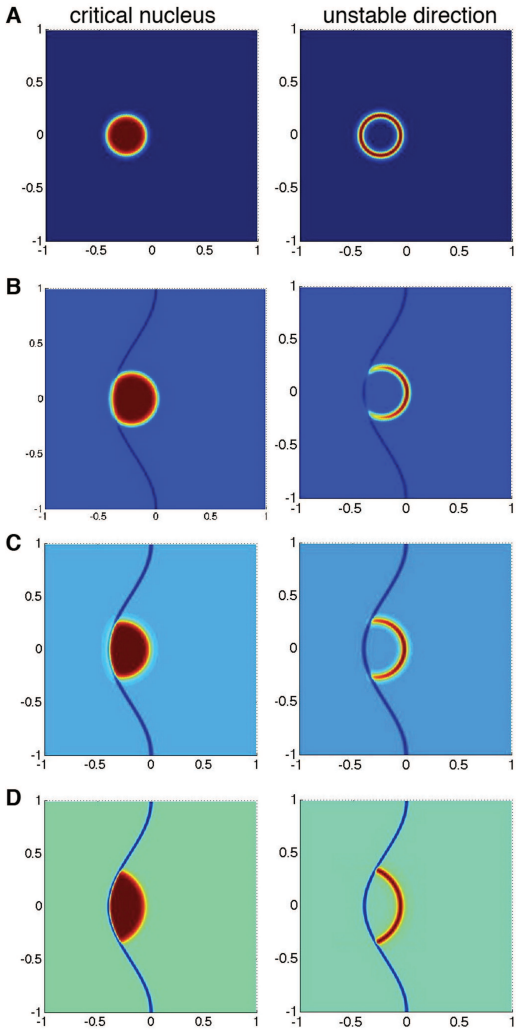


Figure 2: Critical nuclei and unstable directions with different levels of the inhomogeneities near a curve (A) $\gamma=0$, (B) $\gamma=0.2$, (C) $\gamma=0.6$, and (D) $\gamma=1$.

with an isotropic interfacial energy coefficient equaling to $M=0.0004$I. In Fig. 4, we plot a number of possible critical nuclei computed via the SDD with different initial conditions. Because of the complex energy landscape, it is not difficult to see that nucleation can happen at a few possible preferential sites, leading to different shapes of critical nuclei. Meanwhile, the existence of multiple critical nuclei reveals the possibility that the pathway of phase transformation from $\eta=-1$ to $\eta=+1$ in $\Omega$ may contain a few energy barriers so that multiple nucleation events might occur in the complex energy landscape during phase transformation.

We note that the case considered here represents a generic and simplistic description of heterogeneities in real material systems. The method, however, can be applied to more

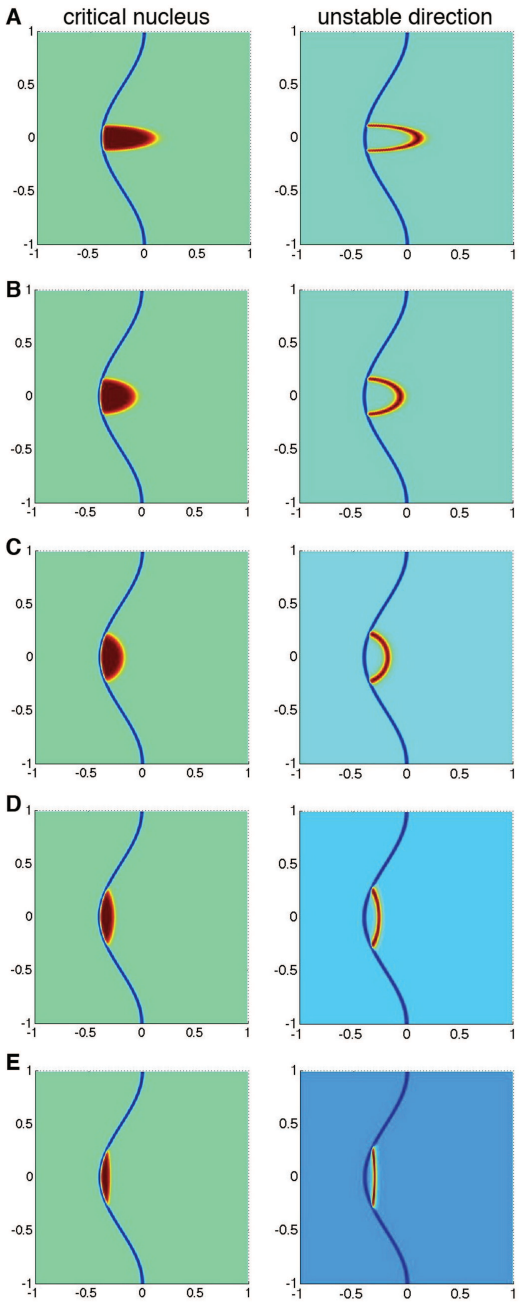


Figure 3: Critical nuclei and unstable directions with interfacial anisotropies near a curve boundary. (A) $a=4$, (B) $a=2$, (C) $a=1$, (D) $a=0.5$, (E) $a=0.25$.

practically interesting cases, by utilization more general phase field models such as those considered in [28].

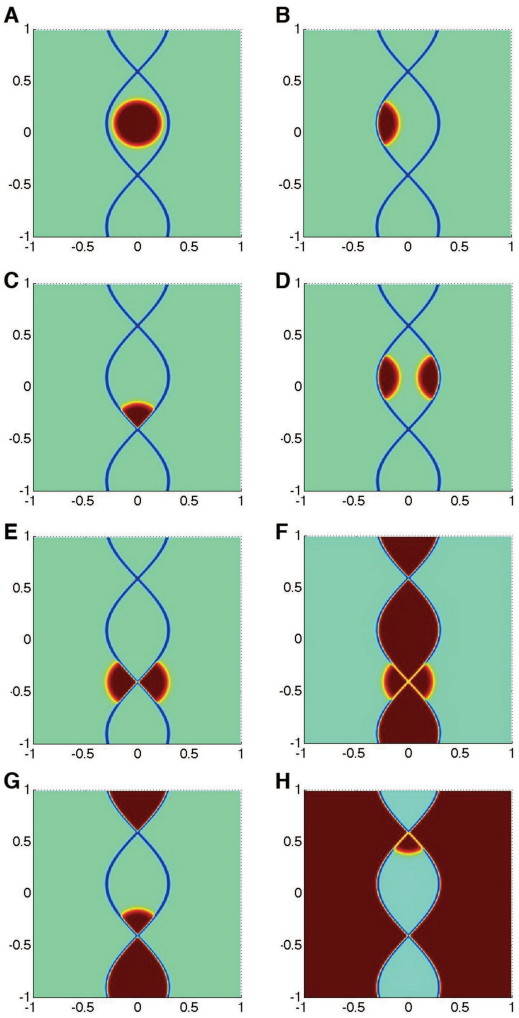


Figure 4: Various critical nuclei in the presence of a self-intersecting curvy phase boundary.

## 4 Precipitate nucleation in FeCr Alloys

In this section we consider nucleation in a real material system related to a particular type of binary alloys, namely, the nucleation of Cr precipitate in FeCr alloys [30]. This serves as an application of GSDD, since the total concentration is set to be a constant. It also allows us to use physically relevant parameters as opposed to the nondimensionalized form used in generic systems considered earlier.

In FeCr alloys, the Cr precipitate is a Cr rich phase with the same structure of the matrix phase. Thus, the Cr concentration can be used to describe the precipitate microstructure in FeCr alloys. We use the phase field model as given in (2.1) but adopt a more conventional notation for variables of interests. Specifically, we consider the Cr

concentration $C_{Cr}(\mathbf{x})$ as a conserved field variable. Then the Fe concentration, $C_{Fe}(\mathbf{x})$, is uniquely determined by $C_{Fe}(\mathbf{x})=1-C_{Cr}(\mathbf{x})$. The total free energy is thus given by

$$E_{total}(C_{Cr})=\int_\Omega\Big(\frac{\kappa}{2}|\nabla C_{Cr}|^2+\frac{NA_0}{\Omega_0}f(C_{Cr},T)\Big)d\mathbf{x}, \tag{4.1}$$

where $N=6.022\times10^{23}$ [atom/mol] is the Avogado's constant, $\Omega_0=1.4087\times10^{-5}$ [$m^3/mol$] is the molar volume for bcc Fe, $\kappa=0.03$ and $A_0=1.602\times10^{-19}$ [J/eV]. These value are taken to be physically meaningful ones. At a given temperature $T$, $f(C_{Cr},T)$ is the free energy density per atom in eV. We take the free energy at $T=600K$ as an illustration [31,32], and find that

$$\begin{aligned}f(C_{Cr},600)=&-4.24652+0.17705C_{Cr}+3.22557C_{Cr}^2-11.1095C_{Cr}^3\\&+18.9389C_{Cr}^4-18.185C_{Cr}^5+9.1486C_{Cr}^6-1.88072C_{Cr}^7\\&+0.051704(1-C_{Cr})\log(1-C_{Cr})+0.051704C_{Cr}\log(C_{Cr}).\end{aligned}$$

In numerical implementation, the conserved Cahn-Hilliard type GSDD does not require extra constraints to be imposed on the concentration variable $C_{Cr}$, and it leads to a time-dependent and spatially fourth-order parabolic equation in $C_{Cr}$. We assume periodic boundary conditions with $\Omega$ being a domain containing a unit period, and set $g(C_{cr})=NA_0f'(C_{cr},T)/\Omega_0$. The Cahn-Hilliard type GSDD is given as follows:

$$\begin{cases}\mu_1\dot{C}_{cr}=-\triangle[\kappa\triangle C_{Cr}-g(C_{cr})]\\\qquad\qquad-\sigma\triangle v\displaystyle\int_\Omega[\kappa\nabla C_{Cr}\nabla v+g(C_{cr})v]\,d\mathbf{x},\\\mu_2\dot{v}=\kappa\triangle v-\dfrac{1}{l}\left(g\Big(C_{cr}+\dfrac{l}{2}v\Big)-g\Big(C_{cr}-\dfrac{l}{2}v\Big)\right)\\\qquad+\dfrac{1}{l|\Omega|}\displaystyle\int_\Omega\left(g\Big(C_{cr}+\frac{l}{2}v\Big)-g\Big(C_{cr}-\frac{l}{2}v\Big)\right)d\mathbf{x}\\\qquad+v\displaystyle\int_\Omega\left[\kappa|\nabla v|^2+\frac{1}{l}\left(g\Big(C_{cr}+\frac{l}{2}v\Big)-g\Big(C_{cr}-\frac{l}{2}v\Big)\right)v\right]d\mathbf{x},\\\mu_3\dot{l}=-l.\end{cases} \tag{4.2}$$

where $\sigma=2$. Obviously, if $\sigma=0$, we recover the conventional Cahn-Hilliard type gradient dynamics from the first equation of (4.2) by setting $l=0$. Note that unlike the case $\sigma=0$ for which the free energy in decreasing in time, the Cahn-Hilliard shrinking dimer dynamics (4.2) allows fluctuations in the free energy so that it goes to the constrained saddle point asymptotically.

It is easy to see that, using the periodic boundary condition, by integrating the first equation of the above GSDD system, we can get the mass conservation of $C_{Cr}$, that is, the conservation of total $C_{Cr}$ concentration is automatically satisfied. Moreover, it is easy to check that if initially we have $v$ to be mean zero and with unit $L^2$ norm, then such properties are preserved at later time.

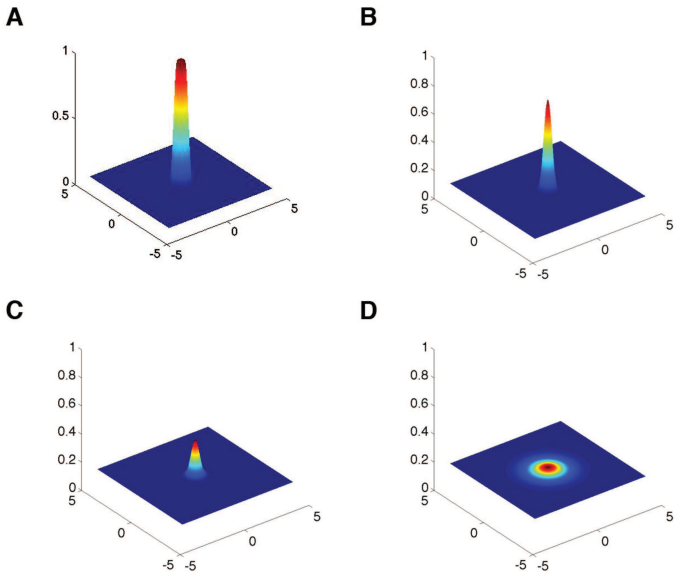


Figure 5: Critical nuclei for 2D FeCr alloys: $C_0 = 0.08$ (A), 0.112 (B), 0.16 (C), 0.2 (D).

Some parameters used in the numerical simulations include the lattice size $l_0 = 0.43nm$. The size of spatial computational domain is $10l_0 \times 10l_0$ in two dimensional space and $10l_0 \times 10l_0 \times 10l_0$ in three dimensional space. The spatial discretization is based on the Fourier spectral methods with grid points being $512 \times 512$ in 2D and $128 \times 128 \times 128$ in 3D, respectively. Numerical verification was conducted to ensure that sufficient resolution has been achieved.

In Fig. 5, we plot the two-dimensional critical nuclei (surface plot of $C_{Cr}$) at different levels of average Cr concentration $C_0 = 0.08, 0.12, 0.16$ and 0.2. As the average Cr concentration increases, the nucleation phase ($C_{Cr} \approx 1$) of the critical nucleus disappears and the interface of critical nucleus becomes more diffuse. Furthermore, an increase of average Cr concentration leads to an exponential decrease of total free energy for nucleation in Fig. 7(A). Notice that the nucleation rate has the form $I = I_0 \exp(-E^*/k_B T)$, with the pre-exponential factor $I_0$ calculated from the fundamental statistical approaches and the Boltzmann's constant $k_B$. It implies that the critical nuclei obtained at large $C_0$ are much more likely to be nucleated.

Next, we compute the critical nuclei for FeCr alloys in three dimensional space and the results of the sliced views are given in Fig. 6. Similar to two-dimensional critical nuclei, the maximum precipitation of critical nucleus decreases as $C_0$ increases. The size of critical nucleus barely changes but the interface diffuses more. Meanwhile, larger average Cr concentration requires lower energy for nucleation shown in Fig. 7(B). The morphologies of critical nuclei and critical energy are critical for capturing the correct growth kinetics of precipitation in FeCr alloys. Further investigations were performed in [32]

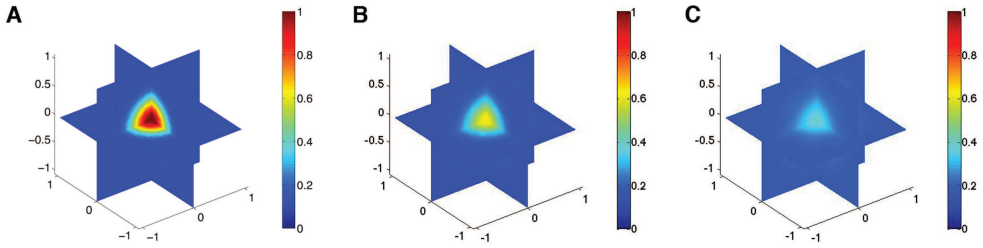


Figure 6: Critical nuclei for 3D FeCr alloys: $C_0 = 0.12$ (A), 0.15 (B), 0.18 (C).

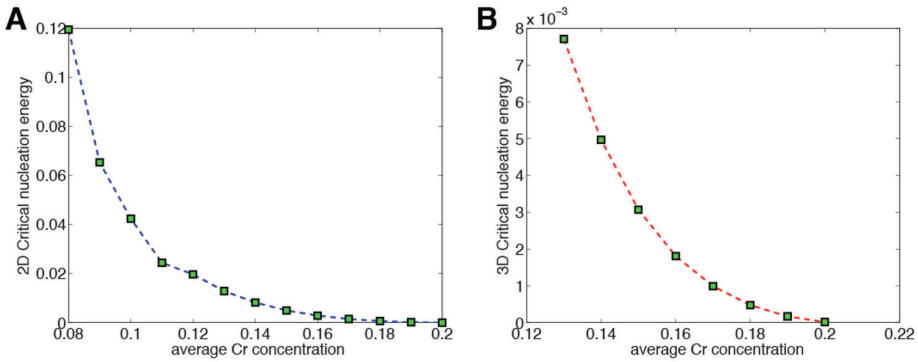


Figure 7: Critical nucleation energy v.s. average Cr concentration in 2D (A) and 3D (B).

for both the critical nuclei obtained by the classical nucleation theory and the critical nuclei obtained by our phase field method, along with discussions on a number of relevant phenomena.

Alternatively, CSDD can be applied to find critical nuclei in FeCr alloys as well. The conservation of the total Cr concentration is a linear constraint on the integral of $C_{Cr}$ over the domain being constant in time so that the action on $C_{Cr}$ of the projection operator onto the constrained space is simply to remove its mean which makes all natural forces having mean zero. The first two equations of the resulting CSDD then become two coupled time-dependent and spatially second-order parabolic systems with $\sigma = 2$. We note that with $\sigma = 0$, the first equation would become an independent equation corresponds to the so-called conserved nonlocal Allen-Cahn or volume-preserving Ginzburg-Landau equation [33].

To compare the performance and efficiency of CSDD (2.8) and GSDD (4.2), we perform a numerical test for FeCr alloys in two dimensional space. We set $C_0 = 0.15$ and use three different initial conditions (a-c) and two different time steps $\tau = 0.005$ and $\tau = 0.01$ in Table 1. The results show that GSDD requires no more than 20% iteration steps of that for the CSDD scheme. In addition, GSDD takes less than 22% CPU time in comparison to CSDD scheme which indicates that the projection step $P(G)$ in CSDD and the additional evaluation of the Laplacian in GSDD consume comparable computation cost

Table 1: Iteration steps and CPU time of CSDD and GSDD for FeCr alloys in 2D.

| | CSDD | | GSDD | |
|---|---|---|---|---|
| | iteration # | CPU (s) | iteration # | CPU (s) |
| (a) $\tau$=0.005 | 554 | 105.7710 | 107 | 22.3770 |
| (b) $\tau$=0.005 | 603 | 115.1633 | 118 | 24.7117 |
| (c) $\tau$=0.005 | 632 | 120.1767 | 125 | 26.2110 |
| (a) $\tau$=0.01 | 281 | 53.5855 | 53 | 11.0877 |
| (b) $\tau$=0.01 | 305 | 58.1790 | 59 | 12.3348 |
| (c) $\tau$=0.01 | 320 | 60.9579 | 62 | 12.9818 |

at each step. Thus, the faster convergence of GSDD than CSDD means that GSDD can significantly save the required CPU time overall.

## 5 Conclusion

In this paper, we applied the shrinking dimer dynamics and generalized shrinking dimer dynamics to phase field models of both heterogeneous nucleations in generic systems and precipitate nucleations in FeCr alloys. We described our approach and conducted a series of numerical simulations to demonstrate its effectiveness. We also compared the different formulations for problems involving a conserved variable. Some interesting observations were revealed. In heterogeneous nucleation, we found that the level of inhomogeneity and complex geometry of phase boundary have significant effects on the morphologies of critical nuclei. The study of nucleation in FeCr alloys also demonstrated that our new approaches are applicable to real materials, and we were able to predict the critical nuclei of Cr precipitation in both two and three dimensional spaces. Meanwhile, we formulated the Generalized Shrinking Dimer Dynamics which can be seen as a saddle point search analog of the generalized gradient flow for energy minimizations. The GSDD includes in particular an analog of the Cahn-Hilliard type dynamics for conserved processes which has not been studied previously in the literature. Naturally, one may utilize the proposed models and algorithms to help implementing the phase field simulation for the study of nucleation and growth kinetics [20]. Thus the current work has laid the foundation to numerical simulations of other complex nucleation processes in the future so as to provide better insights on the role of critical nucleus in various phase transformation processes.

## Acknowledgments

The authors would like to thank Dr. Tae Wook Heo, Dr. Yu Lan Li and Prof. Long-Qing Chen for providing much assistance on the heterogeneous nucleation and FeCr alloys.

This research is supported in part by NSF-DMS 1016073 and 1318586, and the Recruitment Program of Global Youth Experts in China.

**References**

[1] J. Cahn and J. Hilliard, Free energy of a nonuniform system. III. Nucleation in a two-component incompressible fluid, J. Chem. Phys., 31, 688-699, 1959.
[2] H. Schlegel, Exploring potential energy surfaces for chemical reactions: an overview of some practical methods, J. Comput. Chem, 24, 1514-1527, 2003.
[3] D. Wales, Energy landscapes: calculating pathways and rates, International Reviews in Physical Chemistry, 25, 237 - 282, 2006.
[4] L. Zhang, L.-Q. Chen and Q. Du, Morphology of critical nuclei in solid state phase transformations, Phys. Rev. Lett., 98, 265703, 2007.
[5] X.-Y. Cheng, L. Lin, W. E, P.-W. Zhang, and A.-C. Shi, Nucleation of Ordered Phases in Block Copolymers, Phys. Rev. Lett., 104, 148301, 2010.
[6] L. Zhang, L.-Q. Chen and Q. Du, Simultaneous prediction of morphologies of a critical nucleus and an equilibrium precipitate in solids, Comm. Comp. Phys., 7, 674-682, 2010.
[7] G. Henkelman and H. Jönsson, Improved tangent estimate in the nudged elastic band method for finding minimum energy paths and saddle points, J. Chem. Phys., 113, 9978, 2000.
[8] W. E, W. Ren and E. Vanden-Eijnden, String method for the study of rare events, Phys. Rev. B, 66, 052301, 2002.
[9] W. E, W. Ren and E Vanden-Eijnden, Simplified and improved string method for computing the minimum energy paths in barrier-crossing events, J. Chem. Phys., 126, 164103, 2007.
[10] G. Crippen and H. Scheraga, Minimization of polypeptide energy XI. The method of gentlest ascent, Archives of biochemistry and biophysics, 144, 462-466, 1971.
[11] W. E and X. Zhou, The gentlest ascent dynamics, Nonlinearity, 24, 1831-1842, 2011.
[12] G. Henkelman and H. Jönsson, A dimer method for finding saddle points on high dimensional potential surfaces using only first derivatives, J. Chem. Phys., 111, 7010, 1999.
[13] J.Y. Zhang and Q. Du, Shrinking dimer dynamics and its applications to saddle point search, SIAM J. Numer. Anal., 50 (2012), 1899-1921.
[14] G. Henkelman, G. Jöhannesson and H. Jönsson, Methods for finding saddle points and minimum energy paths. In Progress in Theoretical Chemistry and Physics, ed. by W. Lipscomb, I. Prigogine and S. Schwartz, Springer, Dordrecht, 269-302, 2002.
[15] Q. Du and L. Zhang, A constrained string method and its numerical analysis, Comm. Math. Sci., 7, 1039-1051, 2009.
[16] J.Y. Zhang and Q. Du, Constrained shrinking dimer dynamics for saddle point search with constraints, J. Computational Phys., 231, 4745-4758, 2012.
[17] L. Zhang, L.-Q. Chen, and Q. Du, Diffuse-interface description of strain-dominated morphology of critical nuclei in phase transformations, Acta Materialia, 56, 3568-3576, 2008.
[18] L. Zhang, L.Q. Chen, and Q. Du, Mathematical and Numerical Aspects of Phase-field Approach to Critical Morphology in Solids, Journal of Scientific Computing, 37, 89-102, 2008.
[19] L. Zhang, L.-Q. Chen and Q. Du, Diffuse-Interface Approach to Predicting Morphologies of Critical Nucleus and Equilibrium Structure for Cubic to Tetragonal Transformations, J. of Comp. Phys., 229, 65746584, 2010.
[20] T. Heo, L. Zhang, Q. Du and L.-Q. Chen, Incorporating diffuse-interface nuclei in phase-field simulations, Scripta Mater., 63, 8-11, 2010.

[21] R. Backofen and A. Voigt, A phase-field-crystal approach to critical nuclei, J. Phys.: Condens. Matter, 22, 364104, 2010
[22] M. Castro, Phase-field approach to heterogeneous nucleation, Phys. Rev. B, 67, 035412, 2003.
[23] L. Gránásy, T. Pusztai, D. Saylor and J. Warren, Phase Field Theory of Heterogeneous Crystal Nucleation, Phys. Rev. Lett., 98, 035703, 2007.
[24] A.G. Khachaturyan, Theory of Structural Transformations in Solids, Wiley, New York, 1983.
[25] Y. He, Y. Liu, and T. Tang, On large time-stepping methods for the CahnHilliard equation, Applied Numerical Mathematics, 57, 616-628, (2007).
[26] J. Shen and X. Yang, Numerical approximations of Allen-Cahn and Cahn-Hilliard equations, Discrete and Continuous Dynamical Systems, A, 28, 1669-1691, 2010.
[27] S. Y. Hu and L. Q. Chen, Solute Segregation and Coherent Nucleation and Growth near a Dislocation - a Phase-Field Model Integrating Defect and Phase Microstructures, Acta Materialia, 49(3), 463-472, 2001
[28] T.-W. Heo, Phase-field Modeling of Microstructure Evolution in Elastically Inhomogeneous Polycrystalline Materials. PhD diss., The Pennsylvania State University, 2012.
[29] P.Yu, S.Y. Hu, L.Q. Chen, and Q. Du, An iterative perturbation schemes for treating inhomogeneous elasticity in phase field models, with J. Computational Physics, 208, 34-50, 2005
[30] P. J. Grobner, The 885 F (475 C) Embrittlement of Ferritic Stainless Steels, Metall. Trans., 4, 251-260,1973.
[31] Caro, A., Caro, M., Klaver, P., Sadigh, B., Lopasso, E. M., Srinivasan, S. G. , The computational modeling of alloys at the atomic scale: From ab initio and thermodynamics to radiation-induced heterogeneous precipitation. JOM, 59(4), 52-57, 2007.
[32] Yulan Li, Shenyang Hu, Lei Zhang, Xin Sun, Non-classical nuclei and growth kinetics of Cr precipitates in FeCr alloys during aging, Modelling Simul. Mater. Sci. Eng., 22, 025002, 2014.
[33] L. Bronsard, and B. Stoth, Volume-preserving mean curvature flow as a limit of a nonlocal Ginzburg-Landau equation, SIAM Journal on Mathematical Analysis, 28, 769-807, 1997.